20th Australasian Fluid Mechanics Conference
Perth, Australia
5-8 December 2016

Hydrodynamic Measurements on the Joubert Hull in the AMC Cavitation Tunnel with CFD Determined Blockage Corrections

D. B. Clarke[1], D. Butler[1,2], C. L. Ellis[1,2], P. A. Brandner[2]
[1]Maritime Division,
Defence Science and Technology Group, Fishermans Bend, Victoria, 3207, Australia
[2]Australian Maritime College,
University of Tasmania, Launceston, Tasmania, 7250, Australia

Abstract

The Joubert generic submarine geometry and its derivatives are currently the subject of computational studies in over six countries interested in comparing simulation techniques for diesel electric submarine hulls. This paper presents the second set of flow measurements at comparable and higher Reynolds numbers to the existing available measurement set. This new data set allows increased confidence in the use of the Joubert generic submarine geometry for Computational Fluid Dynamic (CFD) studies.

Measurements were taken in the Australian Maritime College's (AMC) cavitation tunnel on the hull of a 1:52 scale generic bare hull Joubert submarine model, oriented at zero degrees incidence. Surface pressure and skin friction measurements were collected at a range of Reynolds numbers. Boundary layer velocity and turbulence intensity surveys were performed at a number of positions aft of the hull. A wake survey was taken at the propeller plane for the bare hull with, and without, the aft control surfaces.

The hull's cross sectional area created an 8.5% solid blockage ratio in the test section. Blockage corrections were performed using CFD simulations of the bare hull as mounted within the test section and additionally in a low blockage domain. The results from these two CFD domains were used to provide full field blockage corrections to the measurements.

Introduction

The Joubert submarine geometry [7] is the focus of a computational and experimental fluid dynamics initiative to study fluid flow around a generic diesel submarine. Measurements of hull static pressures, skin friction and wake velocities were performed in the Australian Maritime College (AMC) cavitation tunnel at higher Reynolds numbers than have been obtained in other facilities to date [1].

The AMC cavitation tunnel is a closed circuit variable pressure water tunnel with a test section that can operate at pressures between 4 kPa and 400 kPa absolute and speeds of 2 m/s to 12 m/s [3]. The 2.60 m long test section has a 0.600 m x 0.600 m cross-section at its entrance. The bottom wall of the test section has a 0.44° slope to compensate for boundary layer growth in order to maintain a constant core velocity in the test section.

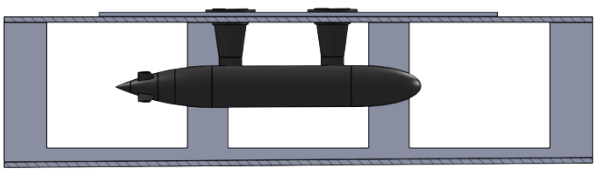

Figure 1. Bare Joubert model with aft control surfaces (AC) mounted in the AMC cavitation tunnel test section.

The bare Joubert hull consists of an ellipsoid nose, cylindrical mid-section and a parabolic stern. The model was machined from aluminium and hard anodised with a surface roughness of less than 0.8 μm. The model was mounted on the test section ceiling via two inline support foils (NACA0016). The Joubert hull has a length, L, of 1350 mm and a maximum diameter of 184.6 mm.

The model features a number of replaceable sections allowing a variety of appendages to be added. The model was mounted with the hull axis 20 mm above the test section centreline (Figure 1). For this series of measurements two configurations were tested; the bare axisymmetric model denoted "bare" in the data, and the bare model with aft control surfaces attached denoted "AC".

The model was fitted with a 'CADcut' adhesive dot trip strip located at a length fraction of x/L=0.05. This location has a minimum estimated momentum thickness Reynolds number (Re_θ) of 230 at the lowest expected Reynolds number of 5.6×10^6. The trip dot height was measured at 92 μm, approximately 150% the boundary layer momentum thickness at that point. The overall solid blockage ratio, including support foils, was estimated at 8.5%.

Measurement Methods

The Joubert submarine model was fitted with 35 surface pressure tappings, 21 on the upper side and 7 on each of the port and starboard sides. The tappings were drilled perpendicular to the surface and were connected via a scanning valve to a Validyne DP15-42 differential pressure transducer, located outside of the test section. The sensor was referenced to the free stream static pressure taken at the test section entrance. Data was sampled at 1024 Hz for 10 s to obtain a mean pressure coefficient (C_P) defined as,

$$C_P = \frac{\overline{P - P_{S\infty}}}{\bar{q}} \tag{1}$$

where P is the surface pressure, $P_{S\infty}$ is the static pressure at the test section entrance and q is the test section inlet dynamic pressure

The skin friction coefficient (C_f) was determined from Preston tube measurements using Head and Ram's calibration [6]. This returns the wall shear as a function of the pressure difference between a Preston tube and the local surface pressure, as per the equation:

$$C_f = \frac{\tau_w}{q} = \frac{f(\bar{P}_{Tube} - \bar{P}_{int})}{\bar{q}} \tag{2}$$

where τ_w is the wall shear stress, P_{Tube} is the pressure at the Preston tube and P_{int} is the surface pressure interpolated to the Preston tube tip location. This calibration does not provide any guidance on its usage on axisymmetric bodies. A reasonable assumption is that the use of this calibration is appropriate when

the local hull radius, R_s, is much larger than the Preston tube diameter.

The Preston tubes were manufactured from thin walled stainless steel tube with an OD and ID of 0.5 mm and 0.4 mm, respectively. The Preston tubes were adhesively mounted via a streamlined plastic fairing over the surface pressure ports (Figure 2). The streamlined plastic fairings were manufactured from acrylic using a 3D printer with a resolution of 16 µm.

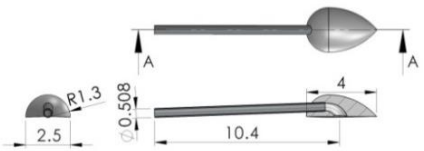

Figure 2. Preston tube and fairing. Units in mm.

Flow velocity was determined from total and static pressure measurements obtained with fast response pressure probes [4] positioned using an automated 3D traverse. Measurements were taken at the same locations with both a static and a total pressure probe head. The 0.7 mm (OD) probe tip was aligned with the test section's axis (*x* direction). The probe housed an Entran EPB-B01-7B-Z2 fast response pressure transducer, measuring the differential between the probe tip and the free-stream static pressure at the test section wall. The instantaneous non-dimensionalised *x* component of the velocity at location "*i*", $(u_{x,i})$, was determined from the total and mean static pressure measurements at that location, as shown in equation (3):

$$\frac{u_{x,i}}{U_\infty} = \sqrt{\frac{P_t - P_s}{q_\infty}} = \sqrt{\frac{P_{t,i} - P_{s\infty}}{q_\infty} - \overline{\left(\frac{P_{s,i} - P_{s\infty}}{q_\infty}\right)}} \qquad (3)$$

where $u_{x,i}$ is the instantaneous x component of velocity at the *i*th location, U_∞ is the test section inlet velocity, P_t is the total pressure at the probe tip, P_s is the pressure measured with the static probe at the same location and $P_{s\infty}$ is the transducer reference static pressure at the test section wall.

For this series of measurements all probe samples were taken at a Reynolds number of 12×10^6 with a 16.4 kHz sampling rate for 20 s. The output of the fast response pressure probe was digitally filtered using a low pass, first order Bessel filter with a 2 kHz cut off frequency.

Boundary layer profiles were measured on the bare hull (Figure 3, top) at four locations along the rear of the model (*x/L*= 0.92, 0.94, 0.96 and 0.98). Circumferential surveys were made in the *x/L*=0.98 plane about the bare and partially appended models (Figure 3, bottom). The radii locations were r/R_{max}=0.3, 0.4, 0.5, 0.6 and 0.7, where R_{max} is the maximum hull radius and r is the radius of the measurement location.

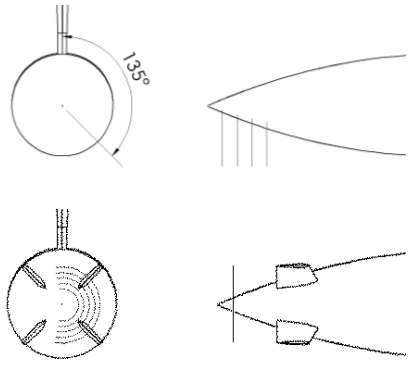

Figure 3. Velocity measurement locations at aft end of the model. Boundary layers (top) and circumferential surveys (bottom).

The distance of the boundary layer measurement from the hull surface was non-dimensionalised by the maximum hull radius ($(r\text{-}R_s)/R_{max}$). The line of measurements approached the submarine normal to its axis and at an angle of 135° relative to the support foils (Figure 3, top). This allowed the probe to travel further out into the free-stream.

The temporal resolution of the fast response pressure probe was sufficient to allow the measurement of the turbulent fluctuations. The single component of the turbulence intensity was then found from equations (3) and (4). The Reynolds Averaged Navier Stokes (RANS) turbulence model used in the CFD modelling does not determine the turbulent component directions and so has been shown as the total turbulent intensity:

$$\frac{u'_{x,i}}{U_\infty} = \frac{\left(u_{x,i} - \bar{u}_{x,i}\right)_{rms}}{U_\infty} = \sigma\left(\frac{u_{x,i}}{U_\infty}\right) \qquad (4)$$

where $u'_{x,i}$ is the x component of unsteady velocity at the *i*th location and σ is the standard deviation.

The unsteady velocity is calculated from the instantaneous total pressure, which is given by:

$$P_T = \frac{\rho}{2}\left((u_x + u'_x)^2 + \left(u_y + u'_y\right)^2 + (u_z + u'_z)^2\right) + \bar{P}_s + p' \qquad (5)$$

where p' the fluctuating component of the static pressure.

If the total head probe, using a squared off tip, is aligned with the flow to within approximately 10°, the total pressure will be correctly measured [2]. If $(u_x + u'_x) \gg (u_y + u'_y)$, $(u_z + u'_z)$ and the probe is aligned with the x axis then only u'_x makes a significant contribution to the unsteady component measured by the probe. Thus when the probe is aligned with the x axis and if the unsteady component of the static pressure is assumed to be negligible:

$$u_x + u'_x \approx \sqrt{2\,(P_T - \bar{P}_S)/\rho}. \qquad (6)$$

The approximation of neglecting u'_y, u'_z and p' should result in a small overestimation of u'_x. This overestimation may increase close to a surface as the reduction in the magnitude of u_x near the wall may result in the condition $(u_x + u'_x) \gg (u_y + u'_y)$, $(u_z + u'_z)$ no longer being met.

CFD Simulation

The CFD domains of the bare hull model with support foils were created to provide novel blockage corrections and increased insight into the flow. These simulations featured the same central geometry, including support foils, with one mesh domain sized to reflect the confined environment of the AMC cavitation tunnel's test section and a second larger, less bounded environment. Both simulations were solved with an inlet velocity set so the Reynolds number based on hull length was 12×10^6. The inlet turbulent intensity and turbulent viscosity ratio were set to 0.5% and 10 respectively. An incompressible RANS solver was used as described by Ellis et al. in a complimentary paper [5]. The low blockage domain featured the same central geometry as the test section domain, with the walls extended outwards to give a solid blockage ratio of 0.49%. Experimental methods of blockage correction, such as measurement of the streamwise pressure gradient on the test section wall, were not used due to the difficulty of obtaining these measurements in the cavitation tunnel.

Results

Surface pressure coefficient distributions are shown in Figure 4. Measurements were also conducted at Reynolds numbers between 6×10^6 and 16×10^6. The surface pressure coefficient distributions for Reynolds numbers at or greater than 10×10^6

showed negligible difference with increasing Reynolds number. A surface pressure coefficient blockage correction was calculated from the difference in surface pressure coefficient, ΔC_p , between the test section and low blockage domain simulations as:

$$\Delta C_p = C_{p\,LB} - C_{p\,TS} \tag{7}$$

where the subscripts *LB* denote the low blockage domain and *TS* the tunnel test section domain. This correction is a function of x/L.

The blockage corrected measurements from the cavitation tunnel in Figure 4 show good agreement with the DST Group low speed wind tunnel data [1]. The tests in both facilities placed boundary layer trips at x/L=0.05. There is a discrepancy with the wind tunnel data at the last measurement location. The wind tunnel results at the last measurement location may have been influenced by their support pylon as the curve shape differs significantly from the other data sets.

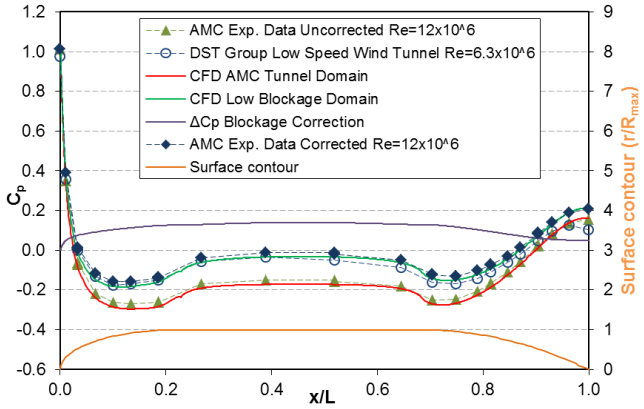

Figure 4. Comparison of surface pressure coefficient distribution for the Joubert geometry from results from the AMC cavitation tunnel, CFD [5] and the DST Group wind tunnel [1]. Uncertainty in C_p ±0.01 for AMC measurements.

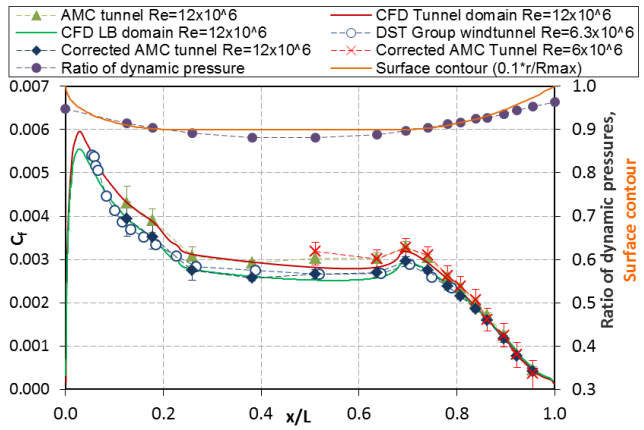

Figure 5. Corrected skin friction compared to the CFD [5] and wind tunnel results [1]. Uncertainties as shown by error bars.

Measured and calculated skin friction is shown in Figure 5. Skin friction is dependent on the boundary layer profile driven by the free stream velocity and surface contour. CFD methods often struggle to accurately calculate wall shear and turbulence, thus comparing the confined and open water CFD measurements was not seen as the best method of correcting for blockage. As the skin friction is sensitive primarily to velocity, a suitable correction is to rescale the measured skin friction coefficients based on the relative maximum velocities between the two CFD models for each x/L position, as in equation (8).

$$C_f = \left(\frac{\tau_w}{q_\infty}\right)_{measured} \left(\frac{max(u_{x,LB})}{max(u_{x,TS})}\right)^2_{CFD} \tag{8}$$

where $max(u_x)$ is the maximum velocity in the x/L plane corresponding to the location measured in the test section; and the measured and CFD subscripts denote data collected from the tunnel and from the CFD models respectively.

The corrected data is in good agreement with the CFD and the wind tunnel data (Figure 5). Skin friction coefficients typically reduce with increasing Reynolds number. The corrected data from the AMC tunnel for Re=12×10^6 is therefore expected to be slightly less than the lower Reynolds number wind tunnel data.

Boundary layer profiles at four locations at the tail are shown in Figure 6. By using the two CFD models it was possible to create a full profile blockage correction for each boundary layer measurement. Typically boundary layers are rescaled based on a reference velocity but this correction fails to account for the change in the boundary layer profile caused by the varying free stream velocity and the increased pressure gradients. The full profile correction is achieved by evaluating the difference between the two CFD domains at the same location as shown in equation (9). This provides an offset for each measured location.

$$\frac{u_{x,i}}{U} = \left(\frac{u_{x,i}}{U_\infty}\right)_{measured} \left(\frac{u_{x,i,\mathrm{LB}}}{u_{x,i,TS}}\right)_{CFD} \tag{9}$$

The subscript i refers to a position in the plane, interpolated from the CFD to the measured location.

The corrected boundary layers show good agreement with the open water CFD in Figure 6. The boundary layers predicted from the CFD are expected to be slightly thicker than the experimentally measured ones, as the modelling assumes turbulent flow along the entire length of the hull. The measured boundary layer was tripped to the turbulent condition at x/L=0.05 and thus had a shorter length over which to grow.

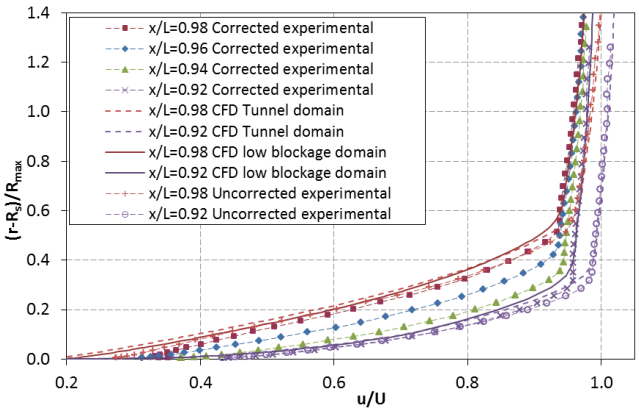

Figure 6. Blockage corrected boundary layer measured velocities for Re=12×10^6 (uncertainty in u/U±0.013) with the extended domain CFD results [5].

The axial component (*x* direction) of turbulence intensity given in Figure 7 was determined from the standard deviation of the velocity as described in equation (4). The increased free-stream velocity causes an increased shear stress, which is distributed across the thickness of the boundary layer. Like skin friction, turbulence intensity is a variable that RANS solvers may struggle to accurately determine, due at least in part to the assumption of homogenous isotropic turbulence. As with the skin friction correction, the turbulence intensity (I_x) measurements were corrected by rescaling the measured data based on the maximum velocity at the *x/L* positions obtained from the CFD models as per the following equation:

$$I_x = \frac{u'_x}{U_\infty} = \left(\frac{u'_x}{U_\infty}\right)_{measured} \left(\frac{max(u_{x,LB})}{max(u_{x,TS})}\right)_{CFD} \quad (10)$$

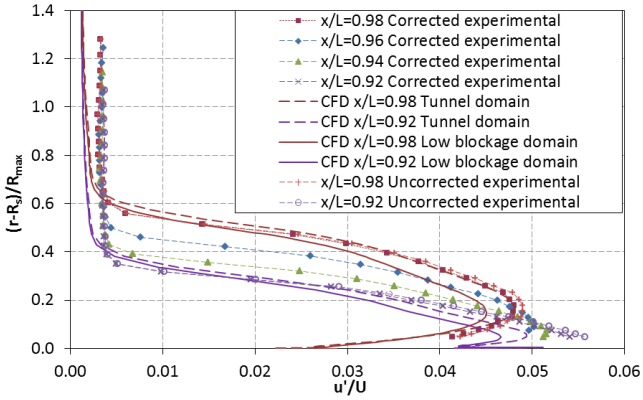

Figure 7. Blockage corrected axial component of boundary layer turbulence intensity for Re=12×10^6 (Uncertainty in u'/U = ± 0.11) with CFD results [5].

The circumferential wake survey velocities and turbulence intensities are shown in Figures 8 and 9. The circumferential wake survey was corrected in the same manner as the boundary layer surveys in equations (9) and (10). These surveys were completed with and without the aft control surfaces. The influence of the aft control surfaces is apparent at 45° and 135° in the results from the circumferential wake survey in Figure 8, along with the wake of the support foils at 180°.

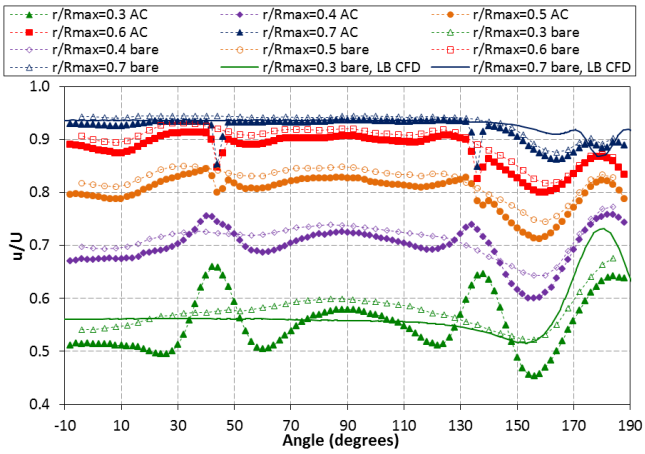

Figure 8. Corrected circumferential survey velocities at *x/L*=0.98 for Re=12×10^6, including selected low blockage CFD results. Uncertainty in *u/U* = ±0.014.

The deficit in the wake behind the control surfaces is apparent in Figure 8 at the greater radial distances, however close to the hull the wake is influenced by the necklace vortices formed at the junction of the control surface and hull. This vortex pulls higher momentum fluid towards the surface of the hull.

A small amount of interaction occurred between the hull wake and the probe arm, resulting a slight curvature of the circumferential survey velocity profile, see the comparison between the results at *r/R*=0.3 and the low blockage CFD in Figure 8. This interaction was not modelled in CFD as the probe arm has a different position for each measurement and so could not be corrected.

Conclusion

Blockage effected measurements of a submarine hull in a cavitation tunnel were successfully rectified by applying corrections based on CFD simulations. The boundary layer and wake surveys complement the data already available for this hull. Where comparable results from other facilities were available this data set showed good agreement.

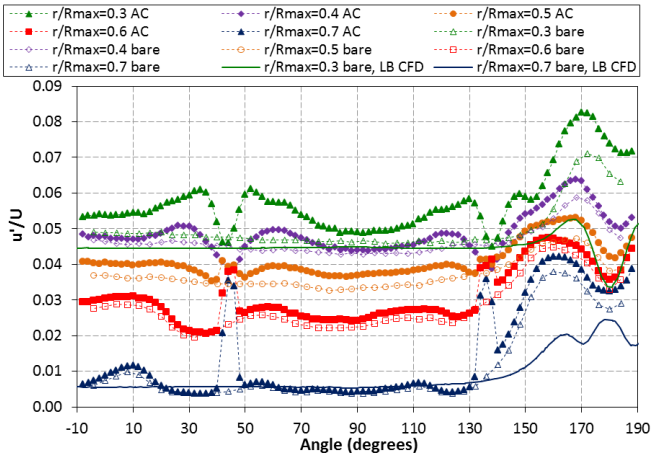

Figure 9. Corrected circumferential survey axial component of turbulence intensity at x/L=0.98 for Re=12×10^6, including selected low blockage CFD results. Uncertainty in u'/U = ± 0.11.

Acknowledgements

The authors would like to acknowledge the efforts of George Jeffs (QinetiQ Pty Ltd) and Michael Popko (QinetiQ Pty Ltd). George undertook the detailed design of the Joubert model used in the AMC cavitation tunnel and Michael manufactured the model.

References

[1] Anderson, B. A., Chapuis, M., Erm, L., Fureby, C., Giacobello, M., Henbest, S., Jones, D., Jones, M., Kumar, C., Liefvendahl. M., Manovski, P., Norrison, D., Quick, H., Snowden, A., Valiff, A., Widjaja and R., Woodjatt, B. Experimental and Computational Investigation of a Generic Conventional Submarine Hull Form, in *Proceedings of the 29th Symposium on Naval Hydrodynamics*, Gothenburg, Sweden: 26-31st August 2012.

[2] Barlow, J.B. Rae, W.H. Pope, A., *Low-Speed Wind Tunnel Testing*, Third Edition; Wiley, 1999

[3] Brandner, P.A. Lecoffre, Y. Walker., G.J., Design Considerations in the Development of a Modern Cavitation Tunnel, in *16th Australasian Fluid Mechanics Conference* Crown Plaza, Gold Coast, Australia 2-7 December 2007

[4] Clarke, D.B. *Experimental and computational investigation of flow about low aspect ratio ellipsoids at transcritical Reynolds numbers*. [PhD Thesis] Launceston, Tas, University of Tasmania. 2009

[5] Ellis, C.L. Clarke, D.B., Butler, D. Complementary CFD Study of Generic Submarine Model Tests in the AMC Cavitation Tunnel, in *20th Australasian Fluid Mechanics Conference*, Perth, Australia 5-18 December 2016

[6] Head, M. R. and Vasanta Ram V. *Improved presentation of Preston tube calibration*. India, Indian Inst. Tech. Kanpur Dept. Aero. Eng. AE-IO/1970. Aeronaut. Q.XXII, 3. 1971

[7] Joubert, P.N., *Some aspects of submarine design. Part 2. Shape of a submarine 2026*; DSTO-TR-1920, Melbourne, Vic., Defence Science and Technology Organisation (Australia). 2006